Single-click beam patterns suggest dynamic changes to the field of view of echolocating Atlantic spotted dolphins (*Stenella frontalis*) in the wild

Frants H. Jensen[1,2*], Magnus Wahlberg[3,4], Kristian Beedholm[5],
Mark Johnson[6], Natacha Aguilar Soto[6,7], Peter T. Madsen[5,8]

[1] Department of Ecology and Evolutionary Biology, Princeton University, Princeton, NJ 08540, USA.
[2] Woods Hole Oceanographic Institution, Woods Hole, MA 02543, USA.
[3] Fjord&Bælt, Margrethes Plads 1, 5300 Kerteminde, Denmark
[4] Marine Biological Research Center, University of Southern Denmark, Hindsholmsvej 11, 5300 Kerteminde, Denmark
[5] Zoophysiology, Department of Bioscience, Aarhus University, 8000 Aarhus, Denmark.
[6] Scottish Oceans Institute, University of St. Andrews, Fife, KY16 8LB, United Kingdom
[7] BIOECOMAC, Dept. Animal Biology, International Campus of Excellence, La Laguna University, La Laguna 38206, Tenerife, Spain
[8] Murdoch University Cetacean Research Unit, School of Veterinary and Life Sciences, Murdoch University, South Street, Murdoch, Western Australia 6150, Australia

Corresponding author:
frants.jensen@gmail.com

Short title: *Biosonar field of view*

Abstract

Echolocating animals exercise an extensive control over the spectral and temporal properties of their biosonar signals to facilitate perception of their actively generated auditory scene when homing in on prey. The intensity and directionality of the biosonar beam defines the field of view of echolocating animals by affecting the acoustic detection range and angular coverage. However, the spatial relationship between an echolocating predator and its prey changes rapidly, resulting in different biosonar requirements throughout prey pursuit and capture. Here we measured single click beam patterns using a parametric fit procedure to test whether free-ranging Atlantic spotted dolphins (*Stenella frontalis*) modify their biosonar beamwidth. We recorded echolocation clicks using a linear array of receivers and estimated the beamwidth of individual clicks using a parametric spectral fit, cross-validated with well-established composite beam pattern estimates. The dolphins apparently increased the biosonar beamwidth, to a large degree without changing the signal frequency, when they approached the recording array. This is comparable to bats that also expand their field of view during prey capture, but achieve this by decreasing biosonar frequency. This behaviour may serve to decrease the risk that rapid escape movements of prey take them outside the biosonar beam of the predator. It is likely that shared sensory requirements have resulted in bats and toothed whales expanding their acoustic field of view at close range to increase the likelihood of successfully acquiring prey using echolocation, representing a case of convergent evolution of echolocation behaviour between these two taxa.

Keywords:

Echolocation, directionality, field of view, perception, dolphin, prey capture

Introduction

Echolocation has evolved in species as diverse as cave birds, microchiropteran bats, and toothed whales (Griffin, 1958; Schevill and McBride, 1956). In contrast to other sensory modalities such as vision or olfaction, echolocation depends on the production of a signal that travels through the environment and is reflected by objects, resulting in returning echoes that are subsequently detected and processed by the echolocating animal (Griffin, 1958). The acoustic field of view of echolocating predators is defined as the area ahead of the predator that is ensonified sufficiently to produce audible echoes (Jakobsen and Surlykke, 2010) and is given by the angular coverage, termed the beamwidth, and the intensity or range of the sonar. The beamwidth and intensity of emitted signals depend on their spectral and temporal properties and on the acoustic behaviour of the echolocating animal (Moss and Surlykke, 2001). There is increasing evidence that bats and toothed whales exhibit significant control over their biosonar (Jakobsen and Surlykke, 2010; Johnson et al., 2008; Moore et al., 2008; Wisniewska et al., 2012) and it is likely that they actively control the perception of their surroundings through changes in biosonar signals and biosonar field of view (Moss et al., 2011).

Biosonar signals are characterised by signal parameters that include source level, duration, centroid frequency, bandwidth, and three-dimensional beam pattern. The source level and beam pattern are of prime importance as they define the functional range and spatial coverage of the biosonar system (Madsen et al., 2007; Urick, 1983). The source level (SL, in dB re 1 µPa @ 1 m for underwater applications) is the sound pressure level measured on the acoustic axis of the biosonar beam at a reference distance of 1 meter from the source (Urick, 1983). The directivity index (DI, in dB) is the difference between the source level of the source in question and the source level of a hypothetical omnidirectional transducer radiating the same acoustic power (Urick, 1983). As the biosonar intensity drops off with increasing off-axis angle, the half-power beamwidth is defined as the angle at which the source level intensity has decreased to half (-3 dB) of the on-axis intensity. Whereas the directivity index is important when discussing sound production efficiency, the beamwidth is a more relevant parameter for understanding how the biosonar system performs in clutter. Focusing the sound energy into a narrow beam restricts the detection of objects to a narrow cone along the axis of the sound beam by increasing their returning echoes and by simultaneously reducing the echoes generated by objects further away

from the axis of the biosonar beam. Directional emission of echolocation signals therefore narrows the acoustic field of view of the echolocating animal, facilitating target detection and discrimination within a restricted area and improving long-range biosonar performance through a higher on-axis source level (Madsen and Surlykke, 2013).

The beamwidth of a biosonar system depends on the dimensions of the sound producing structure and the frequency of the emitted sound so that an increased signal frequency or an enlarged transmitter aperture will result in a narrower biosonar beam (Urick, 1983). The product of the wave number k and the transducer radius a, given as $ka = (2 \pi / \lambda) * a$ is a useful parameter defining the relationship between the effective transducer aperture and the radiated wavelength λ (Au, 1993) with higher directionality achieved through a higher ka number. This means that animals can increase their biosonar beamwidth by either 1) decreasing the frequency of their outgoing sonar signals, or 2) reducing the effective size of the transmitting aperture (Au, 1993).

The amount of control that echolocating animals have over their biosonar beam is remarkable. Microchiropteran bats producing frequency-modulated echolocation signals reduce call amplitude, frequency content and bandwidth during the foraging buzz (Kalko, 1995). Given the relationship between frequency and directionality, this means that microchiropteran bats modify their biosonar directionality and field of view dynamically during prey pursuit and capture by changing biosonar frequency rather than aperture size (Jakobsen et al., 2012; Jakobsen and Surlykke, 2010). Echolocating delphinids studied so far also demonstrate some control over their biosonar beam. Trained delphinids are capable of changing the source level (Moore and Patterson, 1983), frequency content (Moore and Pawloski, 1990), and directionality (Au et al., 1995) of their biosonar signals, and they control their field of view further by steering the beam direction and by controlling the width of the biosonar beam (Finneran et al., 2014; Moore et al., 2008). Most of these adjustable properties may be linked to changes in biosonar frequency, and it is possible that, like in bats, control over the biosonar field of view is primarily a by-product of frequency control. However, a recent study has suggested that trained harbour porpoises may increase their biosonar beamwidth at close range without concurrent changes in signal frequency (Wisniewska et al., 2012). Whether delphinids modify their beam shape strictly through changes

in frequency, as in bats, or may use changes in the size or shape of their sound producing structures to further modify their acoustic field of view remains uncertain, and changes in biosonar beamwidth have yet to be documented from free-ranging animals.

Here we test whether free-ranging Atlantic spotted dolphins (*Stenella frontalis*) can modify the width of their biosonar beam using a new method capable of estimating the beamwidth of individual clicks from vertical hydrophone array recordings. We demonstrate that echolocating Atlantic spotted dolphins seem to increase their field of view when they approach the recording array, and that a significant part of the beamwidth increase must relate to changes in the functional radiation aperture of the melon. Expanding the biosonar field of view at close range may help prevent rapid prey escape responses from taking the prey out of the acoustic field of view of the approaching predator. Our results suggest that both spectral changes to biosonar clicks and morphological changes to the sound generator may contribute to these biosonar dynamics.

Results

We investigated the biosonar field of view using two methods: first, we developed a method for estimating the average (composite) biosonar beam pattern for a series of on-axis echolocation clicks recorded on a one-dimensional array. We then estimated the beamwidth of individual clicks using a parametric fit based on a circular piston model and the amplitude spectra of on-axis clicks recorded across off-axis hydrophones, and we cross-validated these estimates with the composite beamwidth estimate. Finally, we used the parametric spectral fit for estimating the field of view of individual echolocation clicks to show that beamwidth changes as a function of distance from the receiver array, and that these changes are caused in part by changes in frequency, and in part by morphological changes of the sound emitter.

1: Composite beam pattern estimation and method validation

Test trials with two calibrated transducers emitting directional signals were conducted. During both test trials, the transducer was turned gradually along an axis parallel to the axis of the

hydrophone array to simulate the click scans of *S. frontalis* and other species of toothed whales that have been recorded with a linear, vertical array (e.g. Madsen et al., 2004).

To estimate the accuracy of the composite beam pattern, two variants of the same procedure were evaluated. Both variants provided reasonable estimates of the beamwidth (Fig. 1). The traditional error model resulted in negatively biased errors of -19% to -8% beamwidth estimates, whereas the logarithmic error model resulted in smaller errors of -4% to -1% beamwidth estimates (Table 1).

[INSERT TABLE 1 HERE]
[INSERT FIGURE 1 HERE]

Composite beam pattern estimates were surprisingly robust to low sample sizes. Equivalent piston radius (EPR) confidence intervals were consistently wider during simulations with few on-axis clicks, but the mean EPR was highly stable (Fig. 2). The traditional error model for fitting the piston yielded consistently higher EPR estimates (narrower beamwidth) compared to the logarithmic error model (Table 1, Fig. 2). However, this bias was relatively small, in the order of less than half a degree. A similar evaluation of the impact of sample size on data from Atlantic spotted dolphins revealed that EPR estimates recorded with a 6-element hydrophone array were much more robust to low numbers of on-axis clicks, likely because each click was measured across a larger part of the biosonar beam (Fig. 2).

[INSERT FIGURE 2 HERE]

2: Source parameters of *Stenella frontalis* biosonar clicks

A total of 1035 clicks including 28 on-axis clicks were recorded from wild *S. frontalis*. Of these, 19 clicks were recorded within 20 m, with the dolphins milling around the array and often moving in to investigate it. The clicks were typical broadband delphinid echolocation signals (Au, 1993) characterised by short duration and high amplitude (Fig. 3a), with a high centroid frequency and broad bandwidth (Fig. 3b) that corresponds well with the short duration and dominant period in the signal waveform.

[INSERT FIGURE 3 HERE]

The source parameters of these oceanic dolphins were characterised by mean back-calculated apparent source level (±1 s.d.) of 209±4.7 dB re. 1 µPa peak-peak, corresponding to 200±4.6 dB re. 1 µPa rms over a -10 dB envelope time window. The maximum estimated source level was 216 dB re. 1 µPa peak-peak, corresponding to 207 dB re. 1 µPa rms (Table 2). The spectral parameters reflected the broadband nature of these biosonar clicks. Centroid frequency averaged 86±9.0 kHz and centralised RMS bandwidth averaged 33±2.7 kHz, resulting in an average quality factor (Q_{rms}) of 2.6 (Table 2).

[INSERT FIGURE 3 HERE]
[INSERT TABLE 2 HERE]

Using 19 on-axis *S. frontalis* clicks recorded within 20 m, the logarithmic error model estimated an EPR of 5.0±0.20 cm (mean±s.e.m.) with confidence intervals of 4.6 to 5.4 cm (Table 1) for a -3 dB beamwidth of 10.3 degrees in the vertical plane (assuming dolphins were swimming dorsal side up, which seemed to be the predominant swimming orientation for animals near the surface), and a composite DI of 25 dB (BCI: 24.4:25.9 dB) (Table 3). The composite vertical beam pattern and confidence intervals estimated using the logarithmic fitting procedure is shown in Figure 4.

[INSERT FIGURE 4 HERE]
[INSERT TABLE 3 HERE]

Estimates of beamwidth for individual clicks are necessary to understand whether free-ranging animals shape their biosonar beam to different needs. An estimate of the EPR for each click was derived from the parametric spectral fit (Fig. 5). The EPR was 5.1 ± 0.21 (mean ± s.e.m.), with 95% confidence intervals calculated using the percentile bootstrap method of 4.7 to 5.5 cm (Table 3). These results were cross validated with the results from the composite beam pattern estimates, and the two methods corresponded well with each other (Table 3).

The parametric fit revealed that the directionality of the biosonar clicks produced by *S. frontalis* changed with range from the recording array: The EPR, and hence the beamwidth of the animal, correlated significantly with the range of the animal to the hydrophone array (Linear regression: R^2=0.31, F_{17}=7.7, p=0.013, EPR = 0.16 R + 3.15). There was also a significant negative relationship (best fitting slope of -0.06 F_c) between EPR and click centroid frequency in kHz (Linear regression: R^2=0.35, F_{17}=9.0, p=0.008) as would be expected from a relationship between directionality and frequency. We therefore calculated the difference between observed half-power beamwidth and expected half-power beamwidth (given constant EPR and measured centroid frequency of each click), and a negative correlation with range persisted (Linear regression: R^2=0.26, F_{17}=6.04, p=0.02).

[INSERT FIGURE 5 HERE]

[INSERT FIGURE 6 HERE]

Discussion

Echolocating animals exercise a remarkable control over the spectral and temporal properties of their biosonar signals (Kalko and Schnitzler, 1993; Moore et al., 2008; Moore and Pawloski, 1990). Dynamic changes to the acoustic field of view (Jakobsen et al., 2013; Wisniewska et al., 2012) may help echolocating animals inspect their surroundings or lock on to specific targets, shaping the perception of their surroundings via changes in the acoustic gaze (Moss, 2010; Moss et al., 2011). Here we show that wild Atlantic spotted dolphins seem to increase their vertical biosonar beamwidth by some 50% over a four-fold decrease in range. Expanding the acoustic field of view during approach, and especially during prey capture, is likely important to ensure that prey remains within the acoustic field of view despite rapid prey avoidance reactions at close range.

Vertical arrays provide a robust quantification of the composite biosonar beam pattern and the beamwidth of individual clicks

Measuring the biosonar field of view of free-ranging echolocating animals is challenging and requires the use of extensive receiver arrays, acoustic localisation algorithms and conservative

on-axis criteria (Madsen and Wahlberg, 2007; Surlykke et al., 2009). Composite beam patterns, defined as the mean beam pattern of a large series of clicks (Au et al., 1986), have been measured for multiple toothed whale species using linear vertical hydrophone arrays (Kyhn et al., 2010; Kyhn et al., 2009; Wahlberg et al., 2011a; Wahlberg et al., 2011b), but the errors inherent in this estimation procedure have never been addressed. We show that the composite beam pattern of toothed whales, quantified as the mean EPR and corresponding biosonar beamwidth, can be reliably estimated using small sample sizes of on-axis biosonar signals derived from echolocation scans in the wild (Fig. 1) where clicks that are on-axis in the horizontal plane are identified using strict selection criteria. Using a modified fitting procedure from previous studies, beam pattern estimates using a vertical array are both accurate, with 1-4% mean errors compared to known source transducers (Fig. 1), and relatively precise, with 95% confidence intervals of the composite DI spanning 1.5-2.0 dB for the sample sizes used here (Table 1). Given the narrow sonar beam of most toothed whales, studies of beam pattern from wild animals often result in a small number of on-axis clicks (Jensen et al., 2013; Madsen et al., 2004; Wahlberg et al., 2011b). The beam pattern estimates were surprisingly robust to small sample sizes of on-axis clicks for artificial transducers (Fig. 2A) and quick convergence for delphinid signals (Fig. 2B), such that a small sample size will yield a realistic estimate of the biosonar beamwidth as long as the array covers a substantial part of the biosonar beam.

While composite beam pattern estimates may facilitate comparisons of biosonar field of view between species or populations, they are insufficient when addressing causes of variation in the biosonar beam within a dataset. To test whether free-ranging toothed whales such as Atlantic spotted dolphins modify their biosonar beam in the field, we derived an instantaneous estimate of the EPR for individual clicks based on predictable spectral changes (Au, 1993) at increasing off-axis angles (Fig. 5). Cross-validation with the composite beam pattern estimates obtained by fitting a circular piston model with the logarithmic error model indicates that the beam pattern for individual clicks reliably quantifies the biosonar field of view in the plane of the array (Table 3). Thus, using the methods developed here, it is possible to obtain estimates of the beam-pattern of individual clicks, assuming axial symmetry, with a one-dimensional array, and to start teasing apart the underlying mechanisms for variations in acoustic field of view. However, given the assumptions of axial symmetry and reliance on criteria to identify on-axis clicks in the horizontal

plane, two-dimensional planar arrays should be employed where feasible to quantify close-range fine-scale beam patterns.

Free-ranging Atlantic spotted dolphins may increase biosonar field of view at close range

The directionality of biosonar signals allows echolocating animals to detect prey at greater range while reducing the impact of clutter from other nearby but off-axis objects. The broadband biosonar clicks produced by Atlantic spotted dolphins are characterised by a composite DI of 25 dB (Fig. 4), which is very similar to that reported for other similar-sized marine toothed whales (Au et al., 1978; Koblitz et al., 2012; Kyhn et al., 2010; Rasmussen et al., 2004; Wahlberg et al., 2011a). Echolocating toothed whales ranging in size across three orders of magnitude have all evolved highly directional biosonar signals with DIs of 23-32 dB (Koblitz et al., 2012; Madsen and Surlykke, 2013). It has been hypothesised that high directionality has been an important evolutionary driver for high echolocation frequencies in toothed whales (Koblitz et al., 2012), driven by the need for a long-range biosonar system in the marine environment (Jensen et al., 2013; Madsen and Surlykke, 2013). However, while a long biosonar detection range can be advantageous when searching for prey in the open ocean, it may pose other challenges when capturing prey at close range.

Two recent studies have measured changes in the echolocation beam shape and field of view as a function of target range, reaching very different conclusions. Kloepper et al. (2012) reported that a false killer whale, trained to discriminate between objects using echolocation, decreased its biosonar beamwidth by 8% when discriminating between targets at 2.5 m as compared to at 7 m. Even though this change seems counter-intuitive (decreasing SNR at long range where task discrimination is more difficult), the small magnitude of change is unlikely to have an impact on sensory performance. In contrast, harbour porpoises trained to approach and discriminate between two targets showed an increase in beamwidth at close range with more profound sensory implications (Wisniewska et al., 2012).

Here we show that Atlantic spotted dolphins seem to increase their biosonar beamwidth by almost 50% (-3 dB beamwidth from 8 to 12 degrees) when approaching the recording array with a four-fold decrease in range (Fig. 6). The sample size of our study remains very low and it is

likely that a simple linear regression is a poor approximation of how animals modify their acoustic gaze, especially when confronted by live, mobile prey rather than stationary recording arrays. Further lab and field experiments should be performed to verify these results and to tease apart the nature of the relationship between beamwidth and range under different environmental conditions and sensory challenges. However, the increased field of view at short range is comparable to the increasing field of view of trained harbour porpoises (Wisniewska et al., 2012) and bottlenose dolphins (Finneran et al., 2014). This indicates that both phocoenids (family *Phocoenidae*, using narrow-band high-frequency signals) and delphinids (family *Delphinidae*, using broadband biosonar signals) employ a dynamic biosonar beam that allows them to expand their field of view when approaching objects or prey animals, and that these sensory adaptations seem to be important for animals in the wild.

Conformational changes in the melon and surrounding air sacs may help modify the acoustic field of view independently of changes in biosonar frequency

The functional morphology of the structures associated with sound production in toothed whales is highly diverse (Cranford et al., 1996). Echolocation signals in delphinids seem to be produced at the right pair (Madsen et al., 2013b; Madsen et al., 2010) of sound-producing phonic lips (Norris and Harvey, 1972) and are then guided through the dorsal bursae and the fatty tissue of the melon (Cranford et al., 1996). Early studies suggested that the melon functioned as an acoustic lens to concentrate the sound beam (Wood, 1964). It has been suggested that the melon has an acoustic focal point in front of the melon where the acoustic rays converge (Kloepper et al., 2012) but this hypothesis does not take into account that the sound source itself is placed very close to the melon (Cranford et al., 1996). Finite element models based on computed tomography scans of delphinids (Cranford et al., 2013) instead shows that the melon serves as an acoustic collimator. Indeed, several sound propagation simulations have revealed how the skull and associated air sacs provide the structural basis for the frequency-dependent directionality of toothed whale biosonar beams and simultaneously show that the melon may subsequently modify the shape of the biosonar beam (Aroyan et al., 1992; Cranford et al., 2013). While part of the change in beamwidth reported in our study could be explained by the effect of biosonar frequency, variation in biosonar frequency was limited (Table 2, Figure 6) and changes in beamwidth after taking into account the effect of frequency were significant (Fig. 6C). Such

changes could include modifying the geometry of the melon or surrounding air sacs, changing the position of the anterior and posterior bursae, or modifying the actuation of the phonic lips. Both the melon and surrounding air sacs are controlled by complicated epicranial musculature (Cranford et al., 1996; Huggenberger et al., 2009) which likely serves to modify directionality to some degree (Cranford et al., 2013). Similarly, the change in beamwidth that has been observed in the terminal part of prey capture in harbour porpoises also occurred without concurrent spectral changes and has been attributed to conformational changes in the soft structures of the nasal complex (Wisniewska et al., 2012). The extent to which the soft tissue structures in the odontocete forehead may serve to modify directionality defines how much echolocating animals are able to influence their sensory volume. The increase in beamwidth for Atlantic spotted dolphins exceeds 50% (Fig. 6) over a four-fold decrease in range, but the ranges tested do not include the very close target distances that are attained during prey capture attempts, suggesting that greater beamwidth variation is possible. In fact, trained porpoises readily change their beamwidth when investigating an aluminium sphere by 50-100%, and when capturing fish by up to 200% (Wisniewska et al. submitted), demonstrating that the control exercised over their acoustic gaze is quite extensive and may vary significantly depending on the task.

An adaptable acoustic field of view may allow for long-range prey detection while facilitating prey capture at close range

Marine delphinids have likely evolved a highly directional biosonar beam to increase the on-axis source level and thus detection range of possible prey items in the open ocean (Koblitz et al., 2012; Madsen and Surlykke, 2013) and only certain species of freshwater dolphins living in shallow river systems find prey using a short-range, broader biosonar beam (Jensen et al., 2013). Given the high biosonar update rate (typically 1-100 Hz) compared to swim speed (1-5 m/s), it is likely more efficient for an echolocating toothed whale to scan a narrow beam gradually through an environment than it is to swim a greater distance with a shorter but wider biosonar. Blainville's beaked whales depend on significant head-scanning movements of up to ±10 degrees at rates of some 4 degrees per second when searching for prey patches in the deep ocean (Madsen et al., 2013a; Shaffer et al., 2013), demonstrating how a narrow beam can be sequentially scanned through the environment to search a greater volume of water. However, a

narrow beam can be a significant disadvantage when approaching and capturing prey items since rapid escape behaviours at close range might take the prey outside of the acoustic field of view of the approaching predator. Dynamic gaze adjustments, in contrast to a static biosonar beam, allow the approaching predator to increase the width of its field of view during this terminal capture phase, thereby decreasing the likelihood of prey escaping outside the biosonar beam. It is striking that wild delphinids may have comparable gaze adjustment behaviours to trained harbour porpoises (Wisniewska et al., 2012) and echolocating vespertillionid and phyllostomid bats (Brinkløv et al., 2011; Jakobsen and Surlykke, 2010) that all increase their field of view when approaching objects or prey animals. It is likely that shared eco-sensory requirements have led to similar biosonar behaviour in bats and toothed whales to increase the likelihood of successfully acquiring active prey using echolocation, supporting the case of convergent evolution of echolocation behaviour between these highly unrelated lineages.

Conclusion

Free-ranging Atlantic spotted dolphins seem to increase their beamwidth independently of centroid frequency when approaching and investigating a recording array. This demonstrates that wild delphinids are capable of adjusting their outgoing sonar beam independently of frequency, likely using conformational changes of the soft tissue structures in the melon. Bats also expand their field of view when closing in on prey, though by changing frequency rather than aperture. An adaptable biosonar beam offers the benefits of long-range target detection with a narrow beam, while enhancing the capacity for tracking and capturing agile prey by increasing field of view at close range.

Materials and methods

1: Composite beam pattern estimation

Location: Ground-truth experiments were conducted at the Fjord & Baelt research facility in a net pen with a water depth of 3 m. An array of 4 Reson TC4034 hydrophones (Reson, Slangerup, Denmark) spaced 0.75 m apart was suspended horizontally from a floating pontoon at a depth of 1.5 m. Hydrophones were connected through a custom made 4-channel amplification and filtering box (50 dB gain, 10 kHz high-pass filter, 200 kHz low-pass filter) to two synchronised

two-channel National Instruments (National Instruments, Hørsholm, Denmark) USB-6251 analogue-to-digital converters (sampling rate 500 kHz, 16 bit) writing data to a laptop using custom-written LabView (National Instruments, Hørsholm, Denmark) sound acquisition software.

Calibration signals: Directional signals were transmitted 7.6 m from the axis of the horizontal array and at a depth of 1.5 m. Test signals were generated with an Agilent Technologies 33220A arbitrary waveform generator (Agilent Technologies, Hørsholm, Denmark) and emitted through two circular piston transducers of different diameter. First, a 10-cycle, 50 kHz test signal was transmitted through an 18 cm diameter Reson TC2116 transducer (Reson, Slangerup, Denmark) at a rate of 10 pulses per second. Afterwards, a 10-cycle, 150 kHz signal was transmitted through a 12 cm diameter Reson TC2130 transducer (Reson, Slangerup, Denmark), also at a rate of 10 pulses per second. In both cases, the transducer was positioned approximately in front of hydrophone 2 and turned gradually around the axis parallel to the axis of the hydrophone array so that the beam slowly passed back and forth across the array. Although depth constraints in the Fjord&Baelt facility required a horizontally deployed array, the rotation of the transducer around the axis of the array simulated a delphinid scanning its biosonar beam from side to side across a vertically deployed array in the field.

Analysis: Signals were analysed in Adobe Audition 3.0 (Adobe Systems, Inc.) and MatLab 7.0 (MathWorks, Natick, MA, USA) using the same metrics and definitions as for delphinid clicks recorded in the field (Madsen and Wahlberg, 2007). The highest click in each scan was assumed to be pointing towards the axis of the array. The received level on each hydrophone was then calculated as a root-mean-square sound pressure level. The angle of incidence was counted as being within the array aperture if the highest received level was found on one of the inner hydrophones, and the click was discarded from further analysis if this was not the case. Subsequently, the source of the click was localised acoustically using time-of-arrival differences (Spiesberger and Fristrup, 1990) following previous studies (Jensen et al., 2009; Kyhn et al., 2010; Kyhn et al., 2009), after which an initial angle of incidence was calculated to each receiver by assuming that the click was focused on the hydrophone with the highest received level. Then, the theoretical on-axis amplitude and exact angle of incidence relative to the on-axis hydrophone

was calculated by fitting a second-degree polynomial through the three points of angle and amplitude, corresponding to the hydrophone with the highest received level and its two neighbouring hydrophones. The peak of the resulting polynomial located between the three hydrophones was defined as the on-axis direction and amplitude of the biosonar beam. Finally the angles and received levels for all hydrophones were calculated relative to the on-axis angle and amplitude.

Beam pattern estimation: The sonar system of bats and toothed whales is often modelled, for mathematical simplicity, as a flat, circular piston oscillating in an infinite baffle (Au et al., 1978; Strother and Mogus, 1970). Building on this model, the transmission beam pattern was estimated numerically using a parametric intensity fit: First, a waveform of an on-axis signal was identified; here we used the signal with the highest back-calculated source level and no apparent reflections. This model on-axis signal was convolved with the angle-specific impulse response of a circular piston with an EPR from 0.5 cm up to 10 cm in 0.05 cm steps. For each step, the expected sound intensity relative to peak on-axis sound intensity was estimated for off-axis values up to the maximum angle of incidence recorded in the dataset, resulting in a modelled beam pattern for each piston size. These modelled values of relative sound intensity were compared to the estimated angle of incidence and measured sound intensity recorded across all hydrophones (see Kyhn et al., 2010). Two variants of the fitting procedure were tested: In the traditional error model, the best fitting EPR was estimated as the piston model minimising the sum of squared errors between the modelled sound intensity and the measured sound intensity values for all recorded clicks. This reflects the method used in previous studies of odontocete beam patterns using linear arrays (Kyhn et al., 2010; Kyhn et al., 2013; Kyhn et al., 2009; Wahlberg et al., 2011a; Wahlberg et al., 2011b). In the logarithmic error model, the modelled and measured sound intensity values were transformed to a decibel scale ($10 \log_{10}[I/I_0]$ where I_0 is the on-axis intensity) and the best fitting EPR was estimated as the piston model minimising the sum of squared errors between the log-transformed modelled and measured sound intensity values.

Beam pattern confidence intervals: A non-parametric bootstrap method (Efron, 1979) was constructed to evaluate the variation around the beam pattern estimate. Given that on-axis clicks

were derived from different scans, on-axis clicks were assumed to be independent. For a sample size containing N on-axis clicks, individual bootstrap replicates were constructed by randomly sampling N clicks with replacement from the original recorded clicks. In this way, each randomly sampled click included the sound levels recorded across all hydrophones, meaning that this resampling technique is similar to the resampling techniques used for bootstrapping regression. The best-fitting EPR was calculated for each bootstrap as described above. Bootstrap 95% confidence intervals (Efron, 1981) were calculated as the 2.5 and 97.5 percentile of the bootstrap distribution of equivalent piston radii and were confirmed to be similar to the confidence intervals based on a normal distribution (Efron, 1981; Efron, 1982). Confidence intervals for final estimates were based on 2000 bootstrap iterations to facilitate percentile confidence intervals (Manly, 1997).

Effects of sample size: We evaluated the effects of sample size on beamwidth estimates of original datasets using a similar bootstrap method by randomly selecting n clicks out of the available N clicks (sampled with replacement), where n was varied between 2 on-axis clicks up to the total sample size (N), in steps of two. For each sample size, 500 bootstrap iterations were made, and the average (as well as confidence intervals) of the estimated EPR was evaluated from the resulting distribution as described above.

2: Source parameters of *Stenella frontalis* biosonar clicks

Recording habitat: Recordings of Atlantic spotted dolphins (*Stenella frontalis*) were obtained in May 2008 off the west coast of Tenerife, Canary Islands, Spain. Equipment was deployed when encountering groups of spotted dolphins. In several cases, dolphins remained close to the boat for half an hour after stopping the vessel, circling and investigating the vessel and recording array throughout the recording period.

Recording equipment: An array of six Reson TC4034 hydrophones fixed in a hollow PVC tube was suspended vertically between a surface buoy and a 2 kg lead weight. Regular holes in the PVC tube allowed it to fill with water when submerged. The acoustic impedance of the PVC is fairly close to the acoustic impedance of seawater to minimise shadowing and reflections. The top two hydrophones were separated by 1.50 m whereas the remaining hydrophones were

separated by 0.75 m. The top and bottom hydrophones were located at approximately 2 m and 6.5 m depth. A diagram of this recording setup can be found in Kyhn et al. (2010). Hydrophones were connected through two 4-channel amplifier and filtering boxes (1 kHz high-pass, 200 kHz low-pass filter, 40 dB gain) to 3 synchronised 2-channel National Instrument USB-6251 multifunction devices with analogue-to-digital converters running at a sampling rate of 500 kHz, 16 bit per channel. Data were written through USB to a Dell laptop with custom made LabView data acquisition software. Hydrophones were calibrated before and after the field experiments using a B&K 4228 piston-phone calibrator (Brüel & Kjær, Nærum, Danmark). The frequency response of the recording chain was flat (±3 dB) from 1-200 kHz, with a clipping level of 194 dB re. 1 µPa (peak). Data acquisition was initiated and terminated manually, and files were stored approximately every minute.

On-axis criteria: Sound files were analysed with custom-written scripts in MatLab 7.0. An automated click extractor isolated echolocation clicks from each recording and displayed the click amplitudes as a function of time. Given the one-dimensional nature of the array, a set of on-axis criteria following Jensen et al. (2009) was employed to minimise the amount of clicks recorded away from the centre of the biosonar beam. A click was analysed only if it fulfilled the following criteria: i) The click had the highest received level in a scan, i.e. a short series of clicks closely spaced in time and resembling a delphinid moving its beam across the array (normally with increasing and then decreasing signal amplitude). ii) The highest received level of the click was recorded on one of the 4 central hydrophones. iii) The direct path of the click was stronger than any surface reflections present.

Acoustic localisation: The source of signals fulfilling these on-axis criteria was then acoustically localised using time-of-arrival differences of the same click to the 6 receivers (Wahlberg et al., 2001). The signal recorded on the third hydrophone (near the centre of the array), excluding any surface reflections, was cross-correlated with the signals recorded on the remaining hydrophones. The time-of-arrival differences were then found by taking the time of the cross-correlation peak relative to the cross-correlation peak of the first hydrophone, so that time-of-arrival localisation (Spiesberger and Fristrup, 1990) was made with respect to the top hydrophone. An average sound speed of 1524 m/s within the first 40 m water depth was

measured with a CTD (RBR Data Logger model XR-620 CTD, RBR Global, Ontario, Canada). A two-dimensional acoustic localisation (rotationally symmetric around the axis of the array) was obtained as the least-squared solution to the hyperbola equations formed by each time-of-arrival difference and the corresponding difference in receiver coordinates following equations in Madsen and Wahlberg (2007). Signals that could not be localised were dismissed from further analysis. Clicks that were localised more than 50 m away from the array were removed from the analysis following calibration of localisation accuracy (Kyhn et al., 2010) to ensure a localisation error of less than 3 dB in transmission loss (Jensen et al., 2009).

Source parameter estimation: The range from the sound source to each hydrophone was calculated from source coordinates with the Pythagorean equation. The received levels at the hydrophones were calculated as the peak-peak (pp) and root-mean-square (rms) sound pressure levels within a time window given by the -10 dB end points relative to the peak of the amplitude envelope (Au, 1993; Madsen, 2005), which is reasonable given the high signal-to-noise ratio of the on-axis clicks. The duration of clicks was defined as the time interval between -10 dB end points. An energy flux density measure of click amplitude was calculated as the sum of squared sound pressure values within the -10 dB analysis window (Madsen, 2005). The time between the peak of each click and the previous click was defined as the inter-click interval (ICI: Au, 1993). Subsequently, the click amplitude spectrum was calculated as the 3200-points discrete Fourier transform of a 32-point window centred on the peak envelope of each signal. The amplitude spectrum was squared and divided by its peak value to get the normalized power spectrum. The peak frequency, centroid frequency (defined as the frequency separating the power spectrum into two halves of equal energy) and signal bandwidth (centralised RMS bandwidth, -3 dB power and -10 dB power bandwidth) were calculated from this power spectrum, and the quality factor (Q_{rms}) defined as the centroid frequency divided by the centralised RMS bandwidth (Madsen and Wahlberg, 2007). The apparent source level (ASL_{pp}) was defined as the back-calculated sound pressure level 1m from the source at an unknown angle from the acoustic axis (Madsen and Wahlberg, 2007; Møhl et al., 2000) and calculated according to previous studies (e.g. Madsen et al., 2004) by compensating for the transmission loss between source and receiver. Transmission loss was estimated as the sum of spherical spreading ($20 \log_{10}[R]$) and frequency-dependent absorption (αR) over the range R, using a sound absorption coefficient α of 0.02 dB/m at 85 kHz.

548 To quantify the biosonar beam pattern, we then restricted analysis to signals localised closer than
549 20 m to ensure high localization accuracy (standard deviation of less than 2% of range) (Kyhn et
550 al., 2010) and we estimated the composite vertical beam pattern as described above.
551
552 **Single-click beam pattern:** Biosonar clicks exhibit predictable spectral changes when recorded
553 off the acoustic axis (Au, 1993; Au et al., 2012; Wahlberg et al., 2011b). Here we use these
554 changes to estimate the instantaneous EPR from individual clicks using a parametric spectral fit
555 based on a circular piston model. To do this, we extracted the click waveform recorded on all
556 receivers in a 32-point window centred on the peak of the envelope. The click with the highest
557 received level was taken as our best measure of the true on-axis click waveform. We estimated
558 the corrected angle of incidence in the vertical axis using a second-degree polynomial fit as
559 described above, and then calculated the angle of incidence for each receiver. Then, the expected
560 click waveform was modelled for all receivers over a range of simulated circular piston apertures
561 (EPR of 1-10 cm in steps of 0.005 cm). For each piston aperture, the on-axis waveform was
562 convolved with the angle-specific impulse response of a circular piston (eq. 1) at the angle of
563 incidence estimated for each receiver, and the modelled amplitude spectrum obtained through a
564 fast Fourier transform.
565
566 The angle-specific, far-field impulse response of a circular piston was defined (Beedholm and
567 Mohl, 2006) as:

568 $$h(\theta,t) = \frac{4}{\pi T}\sin\left(\cos^{-1}\left[\frac{2t}{T}\right]\right), \text{ with } T = \frac{2a}{c}\sin(\theta) \text{ and defined within } |t| < \tfrac{T}{2} \quad (1)$$

569 Here, c is the sound speed of the medium, a is the piston radius (EPR), and θ is the off-axis angle
570 of each receiver.
571
572 As a measure of the goodness-of-fit of each piston size, we calculated the residual sum of
573 squared error (SSE) between the observed amplitude spectrum and the modelled amplitude
574 spectrum for each receiver. Finally, the best-fitting EPR was estimated as the piston size
575 minimising the total SSE across receivers (Fig. 5). When calculating total SSE, only receivers at
576 angles between 2 and 25 degrees were used to avoid potential frequency-dependent side-lobes,
577 but this proved to have a negligible effect on the final fit.

578

579 The half-power beamwidth (HPBW) was then approximated for each click following (Zimmer et
580 al., 2005):

581 $$HPBW = \frac{185°}{ka} = \frac{185°}{EPR \times 2 \times \pi \times f_c / c_0} \quad (2)$$

582 Where k is the wave number, f_c is the centroid frequency of the click, and a is the radius of a
583 circular piston, approximated here as EPR.

584

585 The parametric fit procedure assumes that the piston is flat and circular. Systematic deviations
586 from this assumption might therefore confound results. To account for this, we also estimated the
587 instantaneous aperture size from predictable spectral changes in biosonar signals recorded off the
588 acoustic axis at a known angle (Au, 1993). Clicks recorded off the acoustic axis are expected to
589 have interference dips in the power spectrum as a function of off-axis angle (lower frequency for
590 greater angles) and aperture dimensions (lower frequency for larger aperture) (Beedholm and
591 Mohl, 2006; Wahlberg et al., 2011b). To avoid the circular piston assumption, we assumed only
592 that the sound emitter was finite along the horizontal axis. For a signal transmitted from a line
593 array with length given by $2a$ (in meters) recorded at an angle θ (in degrees) off the acoustic axis
594 of the array, negative interference will occur at a frequency where the difference in travel
595 distance between signals from the edge and centre of the array equals half the wavelength of the
596 signal. For each receiver, we calculated the one-sided amplitude spectrum (16 points) and then
597 extracted the frequency of the first spectral notch (a local minimum of -1 dB or greater)
598 occurring after the peak frequency (Suppl. Fig. 1). The equivalent piston radius (EPR) was then
599 calculated using the frequency f_n of the first spectral notch, recorded at an off-axis angle θ
600 (estimated for each hydrophone relative to the peak of the polynomial) in a medium with sound
601 speed c_0 (1524 m s^{-1}) as:

602 $$EPR_{notch} = 0.5 \times c_0 \times f_n^{-1} \times \sin(\theta)^{-1} \quad (3)$$

603 Only clicks with S/N ratio greater than 10 dB and recorded at angles greater than 2 degrees and
604 less than 25 degrees were used for this analysis. For each individual click, the estimated EPR
605 was taken as the average estimate across hydrophones. This approach yielded very similar results
606 (Suppl. Fig. 2) compared to the parametric fit, and results are therefore included only in
607 supplementary materials.

Acknowledgements

We would like to acknowledge I. Domínguez, F. Díaz, L. Martinez, C. Aparicio, P. Arranz, C. Gonzalez and P. Aspas for their help during fieldwork. Calibrations were performed with the support of the Fjord&Bælt center in Kerteminde, Denmark. Biosonar clicks of spotted dolphins were recorded under a research permit from the Canary Islands Government granted to La Laguna University. We would like to thank four anonymous reviewers for their constructive feedback on the manuscript.

Funding

The study was funded by frame grants from the Danish Natural Science Foundation to PTM and MW, and by the National Oceanographic Partnership Programme via a research agreement between La Laguna University (NAS) and the Woods Hole Oceanographic Institution (MJ). FHJ was supported by the Danish Council for Independent Research | Natural Sciences, and is currently funded by a postdoctoral fellowship from the Carlsberg Foundation.

Author contributions

FHJ, MW and PTM designed experiments and calibrations. FHJ, KB and MJ developed analytical methods. FHJ, NAS, MJ and PTM acquired funding and conducted fieldwork. FHJ and MW performed method validation experiments. FHJ, MW, KB, NAS, MJ and PTM drafted manuscript.

List of abbreviations

SL Source level

DI Directivity index

EPR Equivalent piston radius

ASL_{pp} Apparent source level, peak-peak

ASL_{rms} Apparent source level, root-mean-square

ASL_{efd} Apparent source level, energy flux density

$Dur_{-10\ db}$ -10 dB envelope duration

638 F_c Centroid frequency
639 BW_{rms} Root-mean-square bandwidth
640 BW_{-3db} -3 dB bandwidth
641 BW_{-10db} -10 dB bandwidth
642 Q_{rms} Root-mean-square quality factor
643 HPBW Half-power beamwidth
644 SSE Sum of squared error
645 BCI Bootstrap confidence interval
646 CI Confidence interval
647

648 Figure captions:

649

650 **Fig. 1: Beam pattern can be accurately estimated using a linear array:** Mean beam pattern
651 estimate of a Reson TC2116 transducer emitting a 50-kHz signal (A) and a Reson TC2130
652 transducer emitting a 150 kHz signal (B) as measured with a 4-hydrophone array. The on-axis
653 sound intensity and angle of incidence from the acoustically localised source to each receiver
654 was estimated through a second-degree polynomial fit (see text). The sound intensity relative to
655 the on-axis intensity is plotted against the angle of incidence for each of 4 receivers recording the
656 same click (squares, colour-coded according to click number). A circular piston model with an
657 aperture minimising the RMS error of received sound intensity on a logarithmic decibel scale
658 (Log method) was fitted to data (dark grey) and 95% confidence intervals for the fit were
659 calculated using a bootstrap method with 2000 replicates (dark grey interrupted lines). The
660 known calibration curve of the transducer is overlaid for comparison (light grey). Note the non-
661 Gaussian error distribution.
662

663 **Fig. 2: Beam pattern estimates are robust to low sample size:** Estimated equivalent piston
664 radius (mean ± 95% bootstrap confidence intervals) as a function of the number of on-axis clicks
665 (ranging from 2 to the total sample size N in increments of 2) included in the piston fitting
666 procedure. Individual clicks recorded on a 4 channel (A) or 6 channel (B) hydrophone array are
667 sampled with replacement from the total population of on-axis clicks (A: N=23, B: N=19) and a
668 piston fitting procedure implemented as described in the text. Means and confidence intervals

were calculated using 500 bootstrap replicates. Note that the baseline grey line for *Stenella frontalis* dataset is based on the best-fitting piston model using the full sample size and logarithmic error model, not on the actual (and unknown) EPR.

Fig. 3: *Stenella frontalis* echolocation clicks: A: Waveform of the 4 echolocation clicks of highest amplitude. Waveforms (sample rate 500 kHz) are upsampled (x10 low-pass interpolation), phase-aligned and normalised to the largest pressure excursion for easier comparison. B: Individual log-transformed power spectra (black lines) and mean *Stenella frontalis* energy distribution (grey dashed line) derived from all on-axis echolocation clicks. Power spectra are constructed using a 320-point fast Fourier transform based on a 32-point (64 µs) window (resulting in x10 sinc interpolation) centered on the peak envelope of each click. Note that the flatness of the mean energy distribution is partly a result of differences in peak frequency between clicks, whereas individual power spectra exhibit much more spectral variation.

Fig. 4: Composite vertical beam pattern of *Stenella frontalis*: Exact angle of incidence was estimated by fitting a second-degree polynomial to data points consisting of the hydrophone recording the highest source level and the two neighbouring hydrophones. A: Apparent source level difference relative to the estimated on-axis source level is shown as a function of angle of incidence (black squares). A piston model (dark grey line) corresponding to an on-axis *Stenella frontalis* click convolved by the angle-specific impulse response of a circular piston with an equivalent piston radius of 5.2 cm was fitted to data. 95% confidence intervals of the estimated beam pattern (Grey interrupted lines) were calculated using a bootstrap method with 2000 replicates. B: Polar plot of estimated vertical beam pattern and 95% bootstrap confidence intervals.

Fig. 5: Equivalent piston radius estimated for an individual biosonar click using a parametric fit: A: Modelled beam pattern for increasing aperture size (solid lines), relative power as a function of absolute angle measured over 6 receivers (red squares), and modelled beam pattern for a 4.57 cm piston (red dashed line). Receiver 3 (shown in subplot B) highlighted. B: Parametric spectral fit: For each receiver, an observed 16-point amplitude spectrum (red

squares) is calculated from the signal waveform. Expected amplitude spectra are calculated by convolving the on-axis signal waveform with the angle-specific impulse response of a circular piston (solid lines, colour-coded according to modelled piston size). C: Individual sum of squared errors for each receiver (coloured lines) and total sum of squared error (black, dashed line) for a signal recorded at a range of 6.4 m and with an estimated EPR of 4.57 cm that minimises the total sum of squared errors across channels.

Fig. 6: Dynamic changes in biosonar field of view for Atlantic spotted dolphins: A: Equivalent piston radius (EPR) (filled circles) estimated for each click through a parametric spectral fit (Fig. 5) and shown as a function of range. Black line represents a significant linear least squares regression (R^2=0.31, F_{17}=7.68, p=0.013) and the grey shaded area represents the 95% confidence interval of the linear regression. B: The half-power beamwidth (HPBW) as a function of range. C: Frequency-independent change in beamwidth: Observed HPBW divided by the HPBW that would be expected if beamwidth was determined by a constant EPR (the mean EPR estimated by the parametric fit method) and a changing centroid frequency (measured for each click). Black line represents a significant linear least squares regression (R^2=0.26, F_{17}=6.04, p=0.02), and the grey, shaded area represents the 95% confidence interval of the linear regression. Data points are colour-coded according to centroid frequency of on-axis click.

Suppl. Fig 1: Implementation of spectral notch estimation of equivalent piston radius (EPR): Solid lines (colour-coded according to estimated angle of incidence) indicate the interpolated (100x) power spectrum derived at each receiver and offset from the on-axis power spectrum by the difference in estimated peak-to-peak source level. Arrows mark the first spectral notch for each channel (notches were estimated from non-interpolated power spectra), with estimated equivalent piston radius calculated from eq. 1. The total mean equivalent piston radius for this click was 4.05 cm.

Suppl. Fig. 2: Dynamic changes in biosonar field of view for Atlantic spotted dolphins estimated using spectral notch approach: A: Equivalent piston radius (EPR) (squares) estimated using the spectral notch method (Suppl. Fig. 1) as a function of range. Black line represents a significant linear least squares regression (R^2=0.44, F_{17}=13.2, p=0.002) and the grey

shaded area represents the 95% confidence interval of the linear regression. B: The half-power beamwidth (HPBW) as a function of range. C: Observed HPBW divided by the HPBW that would be expected if beamwidth was determined by a constant EPR (the mean EPR estimated by spectral notch method) and a changing centroid frequency (measured for each click). Black line represents a significant linear least squares regression (R^2=0.49, F_{17}=16.3, p=0.0008), and the grey, shaded area represents the 95% confidence interval of the linear regression.

Suppl. Fig. 3: Adjustment of apparent source level and interclick interval with range for on-axis Atlantic spotted dolphin biosonar clicks: A: Apparent source level as a function of range (squares), with a log-linear fit to range overlaid (grey line and confidence intervals). B: Interclick intervals as a function of range (squares). Grey line shows the two-way travel time between the dolphin and the array.

References

Aroyan, J. L., Cranford, T. W., Kent, J. and Norris, K. S. (1992). Computer modeling of acoustic beam formation in *Delphinus Delphis*. *Journal of the Acoustical Society of America* **92**, 2539-2545.

Au, W. W. L. (1993). The Sonar of Dolphins: New York: Springer Verlag.

Au, W. W. L., Branstetter, B., Moore, P. W. and Finneran, J. J. (2012). The biosonar field around an Atlantic bottlenose dolphin (Tursiops truncatus). *The Journal of the Acoustical Society of America* **131**, 569-576.

Au, W. W. L., Floyd, R. W. and Haun, J. E. (1978). Propagation of Atlantic bottlenose dolphin echolocation signals. *The Journal of the Acoustical Society of America* **64**, 411-422.

Au, W. W. L. and Herzing, D. L. (2003). Echolocation signals of wild Atlantic spotted dolphin (*Stenella frontalis*). *Journal of the Acoustical Society of America* **113**, 598-604.

Au, W. W. L., Moore, P. W. B. and Pawloski, D. (1986). Echolocation transmitting beam of the Atlantic bottlenose dolphin. *The Journal of the Acoustical Society of America* **80**, 688-691.

Au, W. W. L., Pawloski, J. L., Nachtigall, P. E., Blonz, M. and Gisner, R. C. (1995). Echolocation signals and transmission beam pattern of a false killer whale (*Pseudorca crassidens*). *Journal of the Acoustical Society of America* **98**, 51-59.

Beedholm, K. and Mohl, B. (2006). Directionality of sperm whale sonar clicks and its relation to piston radiation theory. *Journal of the Acoustical Society of America* **119**, EL14-EL19.

Brinkløv, S., Jakobsen, L., Ratcliffe, J. M., Kalko, E. K. V. and Surlykke, A. (2011). Echolocation call intensity and directionality in flying short-tailed fruit bats, *Carollia perspicillata* (Phyllostomidae). *Journal of the Acoustical Society of America* **129**, 427-435.

Cranford, T. W., Amundin, M. and Norris, K. S. (1996). Functional morphology and homology in the odontocete nasal complex: Implications for sound generation. *Journal of Morphology* **228**, 223-285.

Cranford, T. W., Trijoulet, V., Smith, C. R. and Krysl, P. (2013). Validation of a vibroacoustic finite element model using bottlenose dolphin simulations: the dolphin biosonar beam is focused in stages. *Bioacoustics*, 1-34.

Efron, B. (1979). Bootstrap methods: Another look at the Jackknife. *Annals of Statistics* **7**, 1-26.

Efron, B. (1981). Nonparametric standard errors and confidence intervals. *Canadian Journal of Statistics* **9**, 139-158.

Efron, B. (1982). The jackknife, the bootstrap, and other resampling plans. In *CBMS 38, SIAM-NSF*.

Finneran, J. J., Branstetter, B. K., Houser, D. S., Moore, P. W., Mulsow, J., Martin, C. and Perisho, S. (2014). High-resolution measurement of a bottlenose dolphin's (*Tursiops truncatus*) biosonar transmission beam pattern in the horizontal plane. *The Journal of the Acoustical Society of America* **136**, 2025-2038.

Griffin, D. R. (1958). Listening in the dark: the acoustic orientation of bats and men. New Haven CT: Yale University Press.

Huggenberger, S., Rauschmann, M. A., Vogl, T. J. and Oelschlager, H. H. A. (2009). Functional Morphology of the Nasal Complex in the Harbor Porpoise (*Phocoena phocoena* L.). *Anatomical Record* **292**, 902-920.

Jakobsen, L., Kalko, E. V. and Surlykke, A. (2012). Echolocation beam shape in emballonurid bats, *Saccopteryx bilineata* and *Cormura brevirostris*. *Behavioral Ecology and Sociobiology* **66**, 1493-1502.

788 **Jakobsen, L., Ratcliffe, J. M. and Surlykke, A.** (2013). Convergent acoustic field of view in
789 echolocating bats. *Nature* **493**, 93-96.
790 **Jakobsen, L. and Surlykke, A.** (2010). Vespertilionid bats control the width of their biosonar
791 sound beam dynamically during prey pursuit. *Proceedings of the National Academy of Sciences*
792 **107**, 13930-13935.
793 **Jensen, F. H., Bejder, L., Wahlberg, M. and Madsen, P. T.** (2009). Biosonar adjustments to
794 target range of echolocating bottlenose dolphins (*Tursiops* sp.) in the wild. *Journal of*
795 *Experimental Biology* **212**, 1078-1086.
796 **Jensen, F. H., Rocco, A., Mansur, R. M., Smith, B. D., Janik, V. M. and Madsen, P. T.**
797 (2013). Clicking in Shallow Rivers: Short-Range Echolocation of Irrawaddy and Ganges River
798 Dolphins in a Shallow, Acoustically Complex Habitat. *PLoS ONE* **8**, e59284.
799 **Johnson, M., Hickmott, L. S., Soto, N. A. and Madsen, P. T.** (2008). Echolocation behaviour
800 adapted to prey in foraging Blainville's beaked whale (Mesoplodon densirostris). *Proceedings of*
801 *the Royal Society B* **275**, 133-139.
802 **Kalko, E. K. V.** (1995). Insect Pursuit, Prey Capture and Echolocation in Pipistrelle Bats
803 (Microchiroptera). *Animal Behaviour* **50**, 861-880.
804 **Kalko, E. K. V. and Schnitzler, H. U.** (1993). Plasticity in Echolocation Signals of European
805 Pipistrelle Bats in Search Flight - Implications for Habitat Use and Prey Detection. *Behavioral*
806 *Ecology and Sociobiology* **33**, 415-428.
807 **Kloepper, L. N., Nachtigall, P. E., Donahue, M. J. and Breese, M.** (2012). Active
808 echolocation beam focusing in the false killer whale, Pseudorca crassidens. *Journal of*
809 *Experimental Biology* **215**, 1306-12.

Koblitz, J. C., Wahlberg, M., Stilz, P., Madsen, P. T., Beedholm, K. and Schnitzler, H.-U. (2012). Asymmetry and dynamics of a narrow sonar beam in an echolocating harbor porpoise. *The Journal of the Acoustical Society of America* **131**, 2315-2324.

Kyhn, L. A., Jensen, F. H., Beedholm, K., Tougaard, J., Hansen, M. and Madsen, P. T. (2010). Echolocation in sympatric Peale's dolphins (*Lagenorhynchus australis*) and Commerson's dolphins (*Cephalorhynchus commersonii*) producing narrow-band high-frequency clicks. *Journal of Experimental Biology* **213**, 1940-1949.

Kyhn, L. A., Tougaard, J., Beedholm, K., Jensen, F. H., Ashe, E., Williams, R. and Madsen, P. T. (2013). Clicking in a killer whale habitat: Narrow-band, high-frequency biosonar clicks of harbour porpoise (*Phocoena phocoena*) and Dall's porpoise (*Phocoenoides dalli*). *PLoS ONE* **8**.

Kyhn, L. A., Tougaard, J., Jensen, F., Wahlberg, M., Stone, G., Yoshinaga, A., Beedholm, K. and Madsen, P. T. (2009). Feeding at a high pitch: Source parameters of narrow band, high-frequency clicks from echolocating off-shore hourglass dolphins and coastal Hector's dolphins. *Journal of the Acoustical Society of America* **125**, 1783-1791.

Madsen, P. T. (2005). Marine mammals and noise: Problems with root mean square sound pressure levels for transients. *The Journal of the Acoustical Society of America* **117**, 3952-3957.

Madsen, P. T., de Soto, N. A., Arranz, P. and Johnson, M. (2013a). Echolocation in Blainville's beaked whales (*Mesoplodon densirostris*). *Journal of Comparative Physiology a-Neuroethology Sensory Neural and Behavioral Physiology* **199**, 451-469.

Madsen, P. T., Kerr, I. and Payne, R. (2004). Echolocation clicks of two free-ranging, oceanic delphinids with different food preferences: false killer whales *Pseudorca crassidens* and Risso's dolphins *Grampus griseus*. *Journal of Experimental Biology* **207**, 1811-1823.

Madsen, P. T., Lammers, M., Wisniewska, D. and Beedholm, K. (2013b). Nasal sound production in echolocating delphinids (*Tursiops truncatus* and *Pseudorca crassidens*) is dynamic, but unilateral: clicking on the right side and whistling on the left side. *The Journal of Experimental Biology* **216**, 4091-4102.

Madsen, P. T. and Surlykke, A. (2013). Functional convergence in bat and toothed whale biosonars. *Physiology* **28**, 276-283.

Madsen, P. T. and Wahlberg, M. (2007). Recording and quantification of ultrasonic echolocation clicks from free-ranging toothed whales. *Deep-Sea Research Part I - Oceanographic Research Papers* **54**, 1421-1444.

Madsen, P. T., Wilson, M., Johnson, M., Hanlon, R. T., Bocconcelli, A., Aguilar de Soto, N. and Tyack, P. L. (2007). Clicking for calamari: toothed whales can echolocate squid *Loligo pealeii*. *Aquatic Biology* **1**, 141-150.

Madsen, P. T., Wisniewska, D. and Beedholm, K. (2010). Single source sound production and dynamic beam formation in echolocating harbour porpoises (*Phocoena phocoena*). *Journal of Experimental Biology* **213**, 3105-3110.

Manly, B. F. J. (1997). Randomization, bootstrap and Monte Carlo methods in biology. Boca Raton: Chapman & Hall.

Møhl, B., Wahlberg, M., Madsen, P. T., Miller, L. A. and Surlykke, A. (2000). Sperm whale clicks: Directionality and source level revisited. *Journal of the Acoustical Society of America* **107**, 638-648.

Moore, P. and Patterson, S. (1983). Behavior control of echolocation source level in the dolphin (*Tursiops truncatus*). In *Proceedings of the Fifth Biennial Conference on the Biology of Marine Mammals, Boston, MA, The Society for Marine Mammalogy*.

Moore, P. W., Dankiewicz, L. A. and Houser, D. S. (2008). Beamwidth control and angular target detection in an echolocating bottlenose dolphin (*Tursiops truncatus*). *Journal of the Acoustical Society of America* **124**, 3324-3332.

Moore, P. W. B. and Pawloski, D. A. (1990). Investigations on the control of echolocation pulses in the dolphin (*Tursiops truncatus*). In *Sensory abilities of cetaceans: Laboratory and field evidence*, eds. J. A. Thomas and R. A. Kastelein), pp. 305-316. New York: Plenum Press.

Moss, C. F. (2010). Probing the natural scene by echolocation in bats. *Frontiers in behavioral neuroscience* **4**, 33.

Moss, C. F., Chiu, C. and Surlykke, A. (2011). Adaptive vocal behavior drives perception by echolocation in bats. *Current Opinion in Neurobiology* **21**, 645-652.

Moss, C. F. and Surlykke, A. (2001). Auditory scene analysis by echolocation in bats. *Journal of the Acoustical Society of America* **110**, 2207-2226.

Norris, K. S. and Harvey, G. W. (1972). A theory for the function of the spermaceti organ of the sperm whale (*Physeter catodon* L.). In *Animal Orientation and Navigation*, pp. 397-417. Washington, DC: Science and Technology office, NASA.

Rasmussen, M. H., Wahlberg, M. and Miller, L. A. (2004). Estimated transmission beam pattern of clicks recorded from free-ranging white-beaked dolphins (Lagenorhynchus albirostris). *Journal of the Acoustical Society of America* **116**, 1826-1831.

Schevill, W. E. and McBride, A. F. (1956). Evidence for echolocation by cetaceans. *Deep Sea Research (1953)* **3**, 153-154.

Schotten, M., Au, W. W. L., Lammers, M. O. and Aubauer, R. (2004). Echolocation recordings and localization of wild spinner dolphins (*Stenella longirostris*) and pantropical spotted dolphins (*S. attenuata*) using a four hydrophone array. In *Echolocation in Bats and*

Dolphins, eds. J. A. Thomas C. F. Moss and M. M. Vater), pp. 393-400. Chicago: University of Chicago Press.

Shaffer, J. W., Moretti, D., Jarvis, S., Tyack, P. and Johnson, M. (2013). Effective beam pattern of the Blainville's beaked whale (Mesoplodon densirostris) and implications for passive acoustic monitoring. *The Journal of the Acoustical Society of America* **133**, 1770-1784.

Spiesberger, J. L. and Fristrup, K. M. (1990). Passive localization of calling animals and sensing of their acoustic environment using acoustic tomography. *American Naturalist* **135**, 107-153.

Strother, G. K. and Mogus, M. (1970). Acoustical beam patterns for bats: Some theoretical considerations. *The Journal of the Acoustical Society of America* **48**, 1430-1432.

Surlykke, A., Boel Pedersen, S. and Jakobsen, L. (2009). Echolocating bats emit a highly directional sonar sound beam in the field. *Proceedings of the Royal Society B: Biological Sciences* **276**, 853-860.

Urick, R. J. (1983). Principles of underwater sound: Peninsula, Los Altos.

Wahlberg, M., Beedholm, K., Heerfordt, A. and Mohl, B. (2011a). Characteristics of biosonar signals from the northern bottlenose whale, *Hyperoodon ampullatus*. *The Journal of the Acoustical Society of America* **130**, 3077-3084.

Wahlberg, M., Jensen, F. H., Soto, N. A., Beedholm, K., Bejder, L., Oliveira, C., Rasmussen, M., Simon, M., Villadsgaard, A. and Madsen, P. T. (2011b). Source parameters of echolocation clicks from wild bottlenose dolphins (*Tursiops aduncus* and *Tursiops truncatus*). *The Journal of the Acoustical Society of America* **130**, 2263-2274.

Wahlberg, M., Mohl, B. and Madsen, P. T. (2001). Estimating source position accuracy of a large-aperture hydrophone array for bioacoustics. *Journal of the Acoustical Society of America* **109**, 397-406.

Wisniewska, D. M., Johnson, M., Beedholm, K., Wahlberg, M. and Madsen, P. T. (2012). Acoustic gaze adjustments during active target selection in echolocating porpoises. *The Journal of Experimental Biology* **215**, 4358-4373.

Wood, F. G. (1964). Discussion. In *Marine Bio-acoustics Vol II*, (ed. W. Tavolga), pp. 395-396. Oxford: Pergamon.

Zimmer, W. M. X., Johnson, M. P., Madsen, P. T. and Tyack, P. L. (2005). Echolocation clicks of free-ranging Cuvier's beaked whales (*Ziphius cavirostris*). *Journal of the Acoustical Society of America* **117**, 3919-3927.

Tables

Table 1: Validation of composite beamwidth estimation

Values given as means ± s.e.m. (calculated as the standard deviation of the bootstrap distribution of means) and with 95% bootstrap percentile confidence intervals in brackets. Third column represents known values from calibration transducers.

	Traditional error model	**Logarithmic error model**	**Correct**
TC2116 Transducer (50 kHz)	N=23	N=23	
EPR (cm)	**6.95 ± 0.14**	**6.47 ± 0.11**	**6.40**
	[6.63 : 7.15]	[6.28 : 6.73]	
-3 dB Beamwidth (degrees)	**12.7**	**13.7**	**13.8**
	[12.4 : 13.4]	[13.2 : 14.1]	
TC2130 Transducer (150 kHz)	N=12	N=12	
EPR (cm)	**3.11 ± 0.16**	**2.60 ± 0.09**	**2.50**
	[2.75 : 3.29]	[2.50 : 2.79]	
-3 dB Beamwidth (degrees)	**9.86**	**11.8**	**12.2**
	[9.29 : 11.1]	[11.0 : 12.3]	

Table 2: Source properties of echolocation clicks from Atlantic (*Stenella frontalis*) and Pantropical *(Stenella attenuata*) spotted dolphins

	Tenerife, Canary Islands (this study)	**Bahamas** (Au and Herzing, 2003)	**Oahu, Hawaii** (Schotten et al., 2004)
Species	*S. frontalis*	*S. frontalis*	*S. attenuata*
Array type	6-hydrophone vertical	4-hydrophone star	4-hydrophone star
ASL_{pp} (dB re. 1 µPa)	208.8 ± 4.7 (max 216)	(max 223)	212 ± 5
ASL_{rms} (dB re. 1 µPa)	199.6 ± 4.6 (max 207)	-	-
ASL_{efd} (dB re. 1 $\mu Pa^2/Hz$)	150.6 ± 4.3 (max 158)	-	150 ± 4
$Dur_{-10\ dB}$ (µs)	12.8 ± 2.6	-	43 ± 15
F_p (kHz)	78.3 ± 31.0	-	69.4 ± 31.3
F_c (kHz)	85.6 ± 9.0	67.2 ± 25.5	83.4 ± 16.8
BW_{rms} (kHz)	33.1 ± 2.7	36.4 ± 11.0	38.7 ± 6.7
$BW_{-3\ dB}$ (kHz)	91.1 ± 18.9	-	79.8 ± 35.9
$BW_{-10\ dB}$ (kHz)	128.3 ± 8.5	-	-
Q_{rms}	2.6 ± 0.2	-	-
N	28	1277	314

All values in mean ± s.d.

Table 3: Directional properties of Atlantic spotted dolphin (*Stenella frontalis*) echolocation clicks

Method	**Linear Error** (Composite)	**Logarithmic Error** (Composite)	**Parametric fit** (Instantaneous)
EPR (cm)	**5.18 ± 0.23** [4.72 : 5.62]	**4.99 ± 0.21** [4.63 : 5.42]	**5.00 ± 0.27** [4.51 : 5.56]
-3 dB beamwidth (degrees)	**9.86** [9.10 : 10.88]	**10.28** [9.43 : 11.09]	
-10 dB beamwidth (degrees)	**22.05** [20.30 : 24.30]	**22.95** [21.07 : 24.78]	
DI (dB)	**25.5** [24.6 : 26.2]	**25.1** [24.4 : 25.9]	
N	**19**	**19**	**19**

All values given as mean±s.e.m. and with 95% bootstrap confidence intervals in brackets.

Symmetrical -3 dB and -10 dB beamwidth estimated from the beam pattern of the best fitting circular piston model transmitting an on-axis Stenella frontalis biosonar click.

Composite directionality index (DI) calculated as 20 Log10(ka) (Madsen and Wahlberg, 2007).

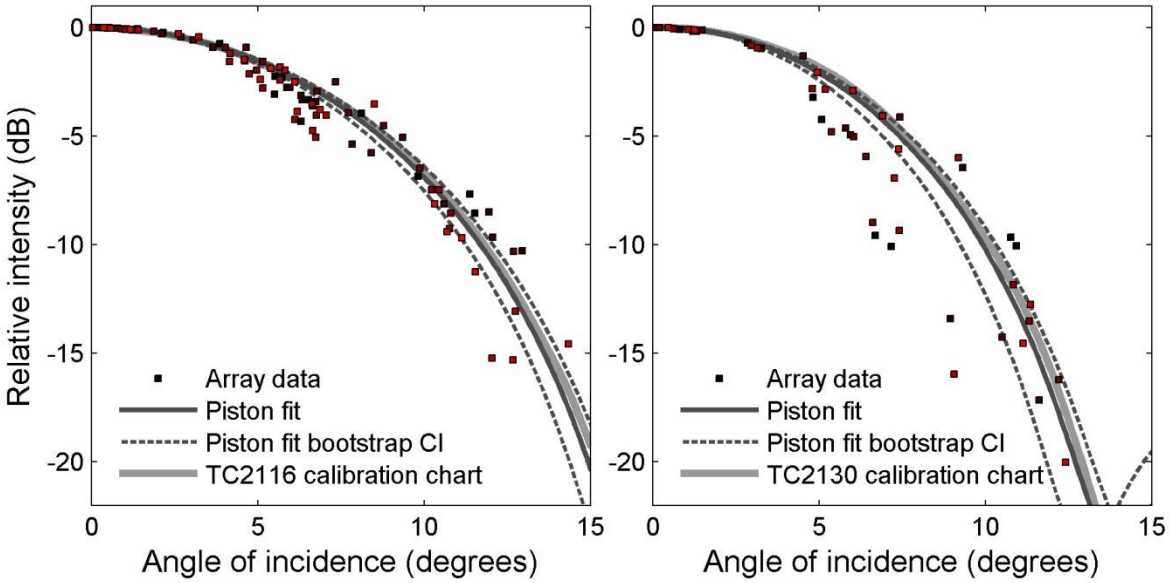
Relative intensity (dB)
0
-5
-10
-15
-20
0
5
10
15
Angle of incidence (degrees)
Array data
Piston fit
Piston fit bootstrap CI
TC2116 calibration chart
Array data
Piston fit
Piston fit bootstrap CI
TC2130 calibration chart

Figure 1

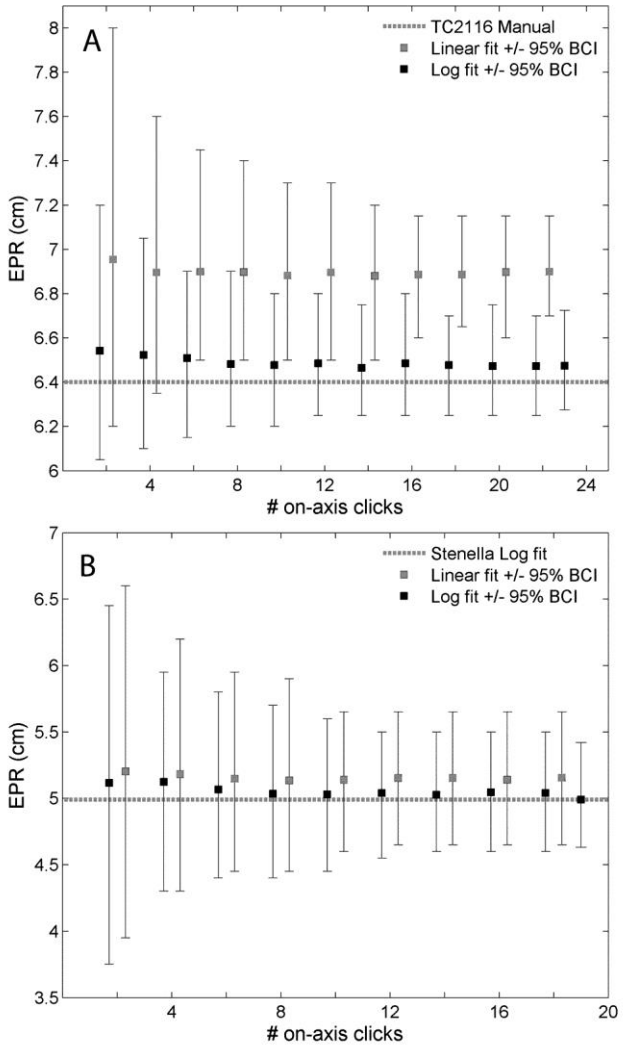
A
TC2116 Manual
Linear fit +/- 95% BCI
Log fit +/- 95% BCI
EPR (cm)
on-axis clicks
B
Stenella Log fit
Linear fit +/- 95% BCI
Log fit +/- 95% BCI
EPR (cm)
on-axis clicks

Figure 2

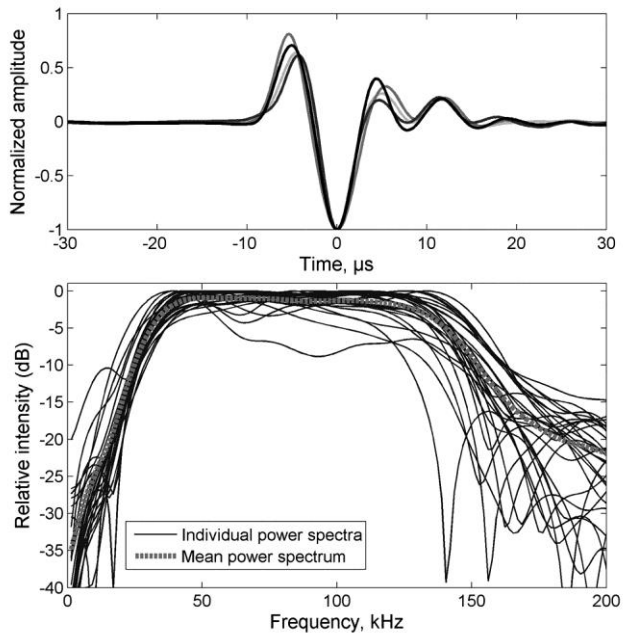
Normalized amplitude
Time, µs
Relative intensity (dB)
Frequency, kHz
Individual power spectra
Mean power spectrum

Figure 3

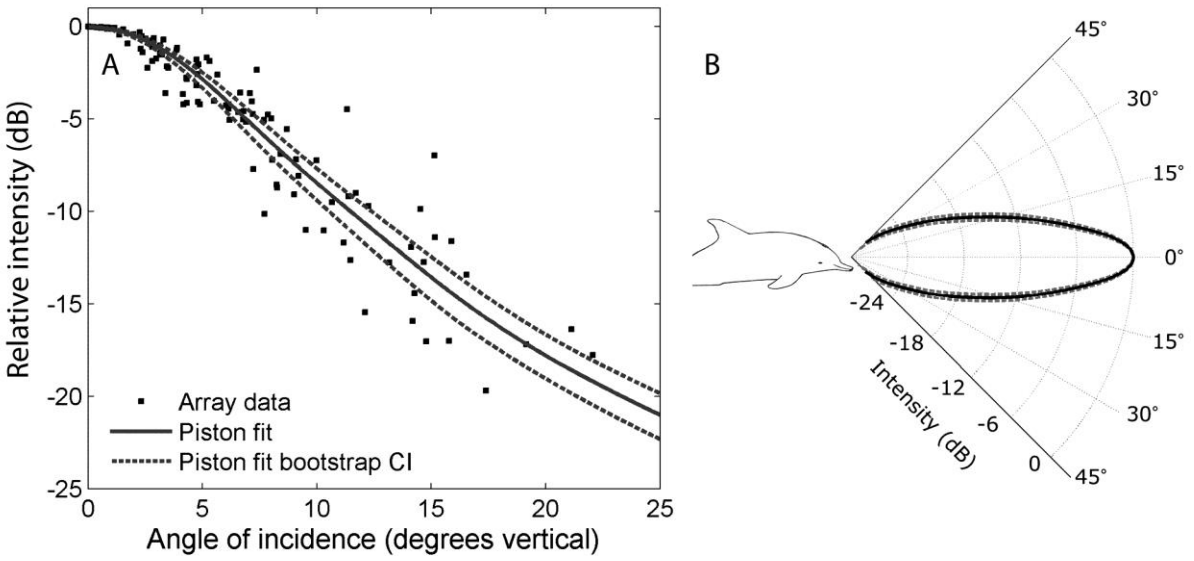
A
Relative intensity (dB)
0
-5
-10
-15
-20
-25
0
5
10
15
20
25
Angle of incidence (degrees vertical)
Array data
Piston fit
Piston fit bootstrap CI
B
45°
30°
15°
0°
15°
30°
45°
-24
-18
-12
-6
0
Intensity (dB)

Figure 4

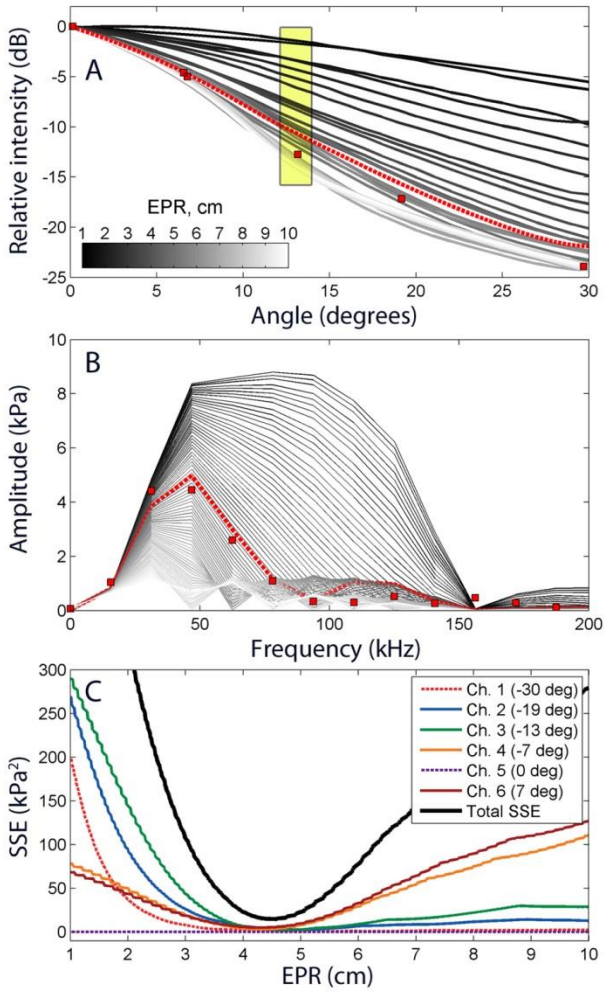
A
Relative intensity (dB)
EPR, cm
1 2 3 4 5 6 7 8 9 10
Angle (degrees)
B
Amplitude (kPa)
Frequency (kHz)
C
SSE (kPa²)
Ch. 1 (-30 deg)
Ch. 2 (-19 deg)
Ch. 3 (-13 deg)
Ch. 4 (-7 deg)
Ch. 5 (0 deg)
Ch. 6 (7 deg)
Total SSE
EPR (cm)

Figure 5

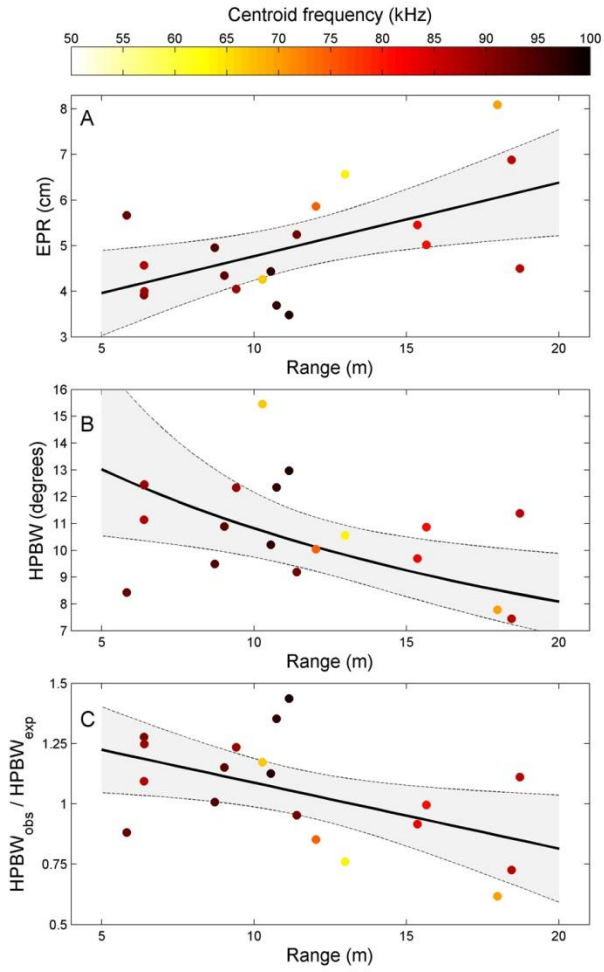
Centroid frequency (kHz)
50 55 60 65 70 75 80 85 90 95 100
A
EPR (cm)
Range (m)
B
HPBW (degrees)
Range (m)
C
HPBW$_{obs}$ / HPBW$_{exp}$
Range (m)

Figure 6